Inorganic Chemistry

Communication

pubs.acs.org/IC

Channel Partition into Nanoscale Polyhedral Cages of a Triple-Self-Interpenetrated Metal–Organic Framework with High CO_2 Uptake

Shuang-Qiu Chen, Quan-Guo Zhai,* Shu-Ni Li, Yu-Cheng Jiang, and Man-Cheng Hu*

Key Laboratory of Macromolecular Science of Shaanxi Province, School of Chemistry and Chemical Engineering, Shaanxi Normal University, Xi'an, Shaanxi 710062, P. R. China

Supporting Information

ABSTRACT: Reported herein is a novel porous metal–organic framework (MOF) exhibiting unique nanoscale cages derived from the 3-fold self-interpenetration of chiral *eta* networks based on trifurcate $\{Zn_2(CO_2)_3\}$ building blocks and 1,3,5-tris(4-carboxyphenyl)benzene ligands. The attractive self-interpenetrated structural features contribute to the highest CO_2 uptake capacity and CO_2 binding ability among the interpenetrated MOFs.

Capturing CO_2 emitted from industrial processes has been an area of intense research. Among the different porous materials investigated for such purposes, crystalline metal–organic frameworks (MOFs) are some of the favorites because of their high surface areas and tunable composition and geometry.[1−5] Usually, the employed strategy to improve the CO_2 uptake capacity in MOFs is to incorporate moieties that have a high affinity for CO_2. Up to now, several factors such as ligand functionalization, unsaturated metal centers, and doping with alkali metals have been studied.[6−8]

In addition to tailoring the functionality of the framework, control over the internal pore size is also important because it has been recognized that a high surface area and a large pore volume do not necessarily lead to a high adsorption capacity for CO_2, especially under ambient conditions. This makes it necessary to develop new synthetic strategies to generate a pore architecture that allows for efficient use of the pore space, for example, through pore-space partitioning of large cage structures, as demonstrated in CPM-5 and CPM-6.[10]

In this aspect, structural interpenetration is of great interest because the degree of interpenetration not only can effectively adjust the pore architecture of MOFs but also may enhance the stability of frameworks through filling of the void space.[10] Undoubtedly, structural interpenetration is closely related to the gas adsorption properties of MOFs. In fact, several interpenetrated structures have shown higher gas sorption capacities for N_2 and H_2 gases than their corresponding noninterpenetrated frameworks.[11−14] However, to our knowledge, the phenomenon of interpenetration in MOFs for CO_2 uptake is far less well studied experimentally because the vast majority of MOFs are noninterpenetrated frameworks. Here we report an interesting zinc carboxylate framework, $[(CH_3CH_2)_2NH_2]$-$[Zn_{12}(SO_3)_2(BTB)_6(HCO_2)_3]\cdot x$DEF [**1**; BTB = 1,3,5-tris(4-carboxyphenyl)benzene, DEF = *N*,*N*-diethylformamide, and $x \approx 15$], which presents a triple self-interpenetration of highly porous *eta* networks. Its most fascinating topological feature is the 1D channel partition via interpenetration into polyhedral cages, which, to the best of our knowledge, represents the first MOF example.

Compound **1** was obtained as brown block crystals via solvothermal reaction of zinc nitrate, Na_2SO_3, and H_3BTB in DEF at 120 °C, which is stable under ambient conditions. The result of X-ray crystal structural analysis reveals that **1** crystallizes in a highly symmetric and yet noncentrosymmetric rhombohedral space group *R*32, in which there are two crystallographically independent Zn^{II} ions, one BTB, one sulfite, and one formate anion in one asymmetric unit, and Zn1 and Zn2 show similar distorted tetrahedral geometries (Figure S1 in the Supporting Information, SI). Three crystallographically independent carboxylate groups of BTB ligands coordinate to the Zn1 and Zn2 centers, forming a trifurcate $[Zn_2(CO_2)_3]$ binuclear secondary building unit (SBU). Although the $[Zn_2(CO_2)_4]$ paddle-wheel SBU is well-known, such a trifurcate $[Zn_2(CO_2)_3]$ SBU is uncommon. As shown in Figure S2 in the SI, each BTB links three trifurcate SBUs through three carboxylate groups, and vice versa. Such a linkage leads to a 3-connected chiral $[Zn_4(BTB)_2]$ framework with 8^3 *eta* topology exhibiting large 1D channels with a dimension of about 2.7 nm (Figure 1a,b). In fact, each 1D channel is formed by a left-handed helical chain extending along the *c*-axis direction, with the helical pitch being 3.4 nm (Figure S3 in the SI). Furthermore, two terminal sites of each trifurcate $[Zn_2(CO_2)_3]$ SBU are occupied by two O atoms from one SO_3^{2-} and one $HCOO^-$, respectively. The S atom is located in a 3-fold axis, and each SO_3^{2-} anion links three adjacent $[Zn_2(CO_2)_3]$ SBUs (Figure S4 in the SI). An interesting 3-fold self-interpenetration of the porous $[Zn_4(BTB)_2]$ frameworks is generated by such a linkage, which divides the large 1D nanochannels into six parts (Figure 1c,d). Each $[Zn_6(CO_2)_9(SO_3)]$ large cluster is surrounded by nine BTB ligands. The whole interpenetrated framework can be simplified as a new 3,9-connected net with the point symbol of $\{4^2.6\}_3\{4^6.6^{27}.8^3\}$ (Figure S5 in the SI).

As shown in Figure 1e, the most fascinating topological feature of **1** is the unique nanoscopic polyhedral cages generated from 3-fold self-interpenetration. Each polyhedral cage is constructed from 8 $[Zn_6(CO_2)_9(SO_3)]$ motifs and 12 BTB ligands. Six $[Zn_6(CO_2)_9(SO_3)]$ motifs are first bridged by six formates to form a regular hexagonal equator plane of the cage; they are further capped by another two $[Zn_6(CO_2)_9(SO_3)]$ clusters through BTB ligands at the top and bottom, respectively. The

Received: September 16, 2014
Published: December 15, 2014

   dx.doi.org/10.1021/ic502254c | *Inorg. Chem.* 2015, 54, 10−12

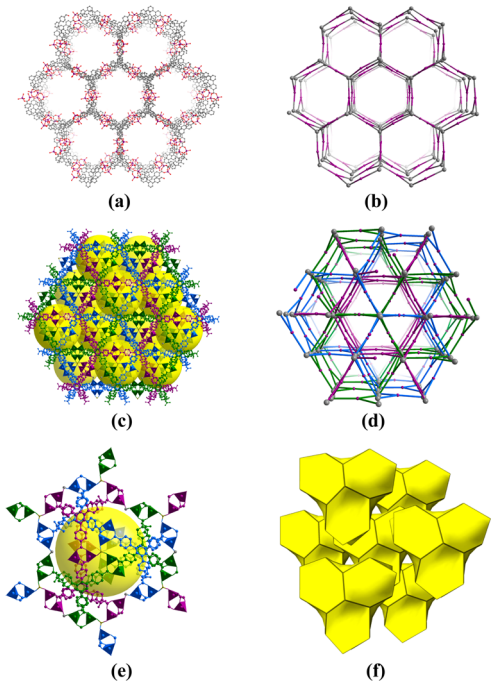

Figure 1. (a) 3-connected $[Zn_4(BTB)_2]$ framework based on trifurcate $\{Zn_2(CO_2)_3\}$ building blocks and BTB ligands. (b) Simplified representation of a 3-connected *eta* chiral network. (c) 3-fold interpenteration of the $[Zn_4(BTB)_2]$ framework. (d) Simplified representation of the 3-fold-interpenetrated framework. (e) Nanoscopic cage enclosed by eight $[Zn_6(CO_2)_9(SO_3)]$ motifs and 12 BTB ligands. (f) Tiles for **1**.

dimension of the hexagonal cavity in the equator plane is about 2.5 nm, and the distance between two capped clusters is about 1.5 nm. This nanosized cage can be simplified as a squeezed hexagonal bipyramid if we just take the large $[Zn_6(CO_2)_9(SO_3)]$ SBUs into account (Figure S6 in the SI). A total of triangular windows with dimensions of about 18.2 × 20.5 × 17.8 Å^3 are observed for the polyhedron. Each hexagonal-bipyramidral cage serves as a supermolecular building block (SBB) linking six adjacent SBBs to extend an overall 3D structure of **1** (Figures 1f and S6 in the SI). Although a number of polyhedral MOFs have been reported, so far there are no examples of the 3D polyhedral framework introduced by self-interpenetration.

Because the cages of **1** are generated from the channel partition through 3-fold self-interpenetration, the original nanochannels of *eta* networks are partly blocked. However, such an interpenetration may be beneficial to H_2 and CO_2 uptakes because large pores do not necessarily lead to high uptake capacities for small molecules. On the other hand, interpenetration has minimized the empty space, which could significantly enhance the stability of the frameworks. Therefore, we hypothesized that this novel triple-interpenetrated compound should be stable and permanently porous. Indeed, thermogravimetric analysis (TGA) shows that the removal of solvent molecules occurs in the temperature range of 40−150 °C. The self-interpenetrated framework of **1** can be stable to about 380 °C (Figure S7 in the SI). In addition to partitioning the above channel into a cage topological feature, **1** is also a charged framework, which may generate an electric field across the pore space to enhance the solid−gas interactions. Overall, the aforementioned interesting features (e.g., triple interpenetration, channel partition, nanoscopic polyhedral cages, and charged framework) encourage us to explore its gas uptake ability.

PLATON calculations indicate that the 3-fold-self-interpenetrated framework **1** still has a total solvent-accessible volume of 16719 Å^3, which occupies approximately 64.7% of the volume of the whole crystal. The architectural stability and permanent porosity were also confirmed by measuring the gas adsorption measurements (N_2, H_2, and CO_2) by a Micromeritics ASAP 2020HD88 surface-area and pore-size analyzer. No sample activation was applied, and the as-synthesized sample was directly degassed at 80 °C for 48 h under a vacuum prior to the measurement. Interpenetrated framework **1** exhibits a type I adsorption isotherm typical of materials of permanent microporosity. The Langmuir and Brunauer−Emmett−Teller (BET) surface areas were 1118 and 781 m^2/g, respectively (Figure 2a). A micropore volume of 0.386 cm^3/g (Horvath−Kawazoe method) and a median pore size of 15.86 Å were also calculated.

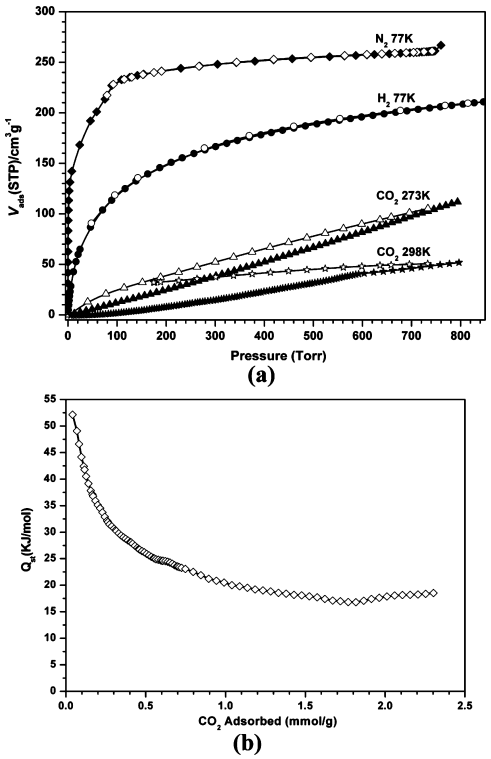

Figure 2. (a) N_2 and H_2 isotherms of **1** at 77 K and CO_2 isotherms at 273 or 298 K. (b) Enthalpy of adsorption (Q_{st}) as a function of the CO_2 uptake.

The accessible porosity confirmed by the N_2 sorption study prompts us to further investigate the gas sorption properties of H_2 and CO_2. The uptake of H_2 at 1 atm and 77 K is 1.84 wt % (205.6 cm^3/g; Figure 2a), which is comparable to those of previously reported MOFs such as Co-MOF-74,[15] IRMOF-3,[16] and CPM-6[10] and outperforms some well-known MOFs and ZIFs like MOF-177,[17] Zn-MOF-74,[16] Bio-MOF-1,[18] and ZIF-8.[19] If just the interpenetrated MOFs are taken into account, the H_2 adsorption capacity of **1** is basically equal to the uptake of a 2-fold-interpenetrated MOF Cd-ANIC-1[20] and comparative to the uptake of a well-known interpenetrated MOF (PCN-6)[13] with a similar triangular carboxylate ligand (1.74 wt % activated at 50 °C and 1.9 wt % activated at 150 °C). However, the 3800 m^2/g BET surface area of PCN-6 is much larger than that of **1**. Although Cd-ANIC-1 has a much smaller BET surface area, amino functionalization may help to improve the gas uptake. Compared

dx.doi.org/10.1021/ic502254c | *Inorg. Chem.* 2015, 54, 10−12

with some other interpenetrated MOFs, such an amount of H_2 adsorption for compound **1** is on the top of the list (Table S2 in the SI).

Self-interpenetrated framework **1** also exhibits a high CO_2 uptake capacity of 108.8 cm^3/g (4.86 mmol/g) at 273 K and 1 atm (Figure 2a). At room temperature (298 K) and 1 atm, it has a CO_2 uptake of 50 cm^3/g (2.23 mmol/g). Notably, the CO_2 adsorption capacity at 273 K and 1 atm nearly outperforms all previously reported interpenetrated MOFs (Table S2 in the SI) such as SNU-71,[21] NOTT-202,[22] and YO-MOF.[23] Although the amino-functionalized, interpenetrated Cd-ANIC-1 shows the same H_2 uptake ability, its CO_2 adsorption capacity (4.72 mmol/g, 273 K, 1 atm) is lower than that of **1**. Compared to the noninterpenetrated MOFs, although complex **1** has a lower CO_2 uptake than Mg-MOF-74[16] and other limited best CO_2 uptake MOFs,[24−26] the CO_2 adsorption capacity still outperforms many famous noninterpenetrated porous compounds such as TMA@Bio-MOF-1,[27] ZIF-78,[28] and ZIF-69[29] at 273 K and 1 atm.

The isosteric heat of adsorption (Q_{st}) of CO_2 for **1** was further predicted from the Clausius−Clapeyron equation based on simulated adsorption isotherms at 273 and 298 K. At zero loading, a maximum value of 52.5 kJ/mol indicates a strong interaction of CO_2 with the 3-fold-interpenetrated framework. Such a large Q_{st} value is just smaller than those of limited MOFs, such as MIL-100[29] and amino-functionalized $H_3[(Cu_4Cl)_3(BTTri)_8]$,[30] and surpasses most of the reported MOFs like MOF-5,[31] HKUST-1,[32] and Bio-MOF-1.[33] Clearly, the triple interpenetration into nanoscopic polyhedral cages and charged frameworks contributes significantly to its high CO_2 uptake.

In conclusion, the triple self-interpenetration of porous *eta* networks leads to an exceptional porous material in which nanoscale hexagonal-bipyramidral polyhedral cages are generated. Such a self-interpenetration architecture partitions the large pore space into small domains, which effectively enhances the interaction between the framework and gas molecules. The integrated structural features (i.e., framework catenation, channel partition, nanoscopic cages, and charged framework) contribute to not only the highest CO_2 uptake capacity but also the strongest CO_2 affinity among the interpenetrated MOFs.

■ ASSOCIATED CONTENT

Ⓢ Supporting Information

Detailed experimental and crystallographic (in CIF format) data, figures showing structural details, X-ray diffraction patterns, a TGA curve, and Fourier transform infrared spectra. This material is available free of charge via the Internet at http://pubs.acs.org.

■ AUTHOR INFORMATION

Corresponding Authors

* E-mail: zhaiqg@snnu.edu.cn.
* E-mail: hmch@snnu.edu.cn.

Notes

The authors declare no competing financial interest.

■ ACKNOWLEDGMENTS

This work was supported by the National Natural Science Foundation of China (Grant 21271123), the New Century Excellent Talents in University (Grant NCET-12-0897), and the Natural Science Foundation of Shaanxi Province (Grant 2014KJXX-50).

■ REFERENCES

(1) Férey, G. *Chem. Soc. Rev.* **2008**, *37*, 191−214.
(2) Koh, K.; Wong-Foy, A. G.; Matzger, A. J. *J. Am. Chem. Soc.* **2009**, *131*, 4184−4185.
(3) Yuan, D.; Zhao, D.; Sun, D.; Zhou, H. C. *Angew. Chem., Int. Ed.* **2010**, *49*, 5357−5361.
(4) Deng, H.; Doonan, C. J.; Furukawa, H.; Ferreira, R. B.; Towne, J.; Knobler, C. B.; Wang, B.; Yaghi, O. M. *Science* **2010**, *327*, 846−850.
(5) Furukawa, H.; Ko, N.; Go, Y. B.; Aratani, N.; Choi, S. B.; Choi, E.; Yazaydin, A. O.; Snurr, R. Q.; O'Keeffe, M.; Kim, J.; Yaghi, O. M. *Science* **2010**, *329*, 427−428.
(6) Mason, J. A.; Veenstr, M.; Long, J. R. *Chem. Sci.* **2014**, *5*, 32−51.
(7) Chaemchuen, S.; Kabir, N. A.; Zhou, K.; Verpoort, F. *Chem. Soc. Rev.* **2013**, *42*, 9304−9332.
(8) Sumida, K.; Rogow, D. L.; Mason, J. A.; McDonald, T. M.; Bloch, E. D.; Herm, Z. R.; Bae, T. H.; Long, J. R. *Chem. Rev.* **2012**, *112*, 724−781.
(9) Li, J.-R.; Sculley, J.; Zhou, H.-C. *Chem. Rev.* **2012**, *112*, 869−932.
(10) Zheng, S. T.; Bu, J. T.; Li, Y.; Wu, T.; Zuo, F.; Feng, P.; Bu, X. *J. Am. Chem. Soc.* **2010**, *132*, 17062−17064.
(11) Jiang, H. L.; Makala, T. A.; Zhou, H. C. *Coord. Chem. Rev.* **2013**, *257*, 2232−2249.
(12) Ma, S.; Eckert, J.; Forster, P. M.; Yoon, J. W.; Hwang, Y. K.; Chang, J.-S.; Collier, C. D.; Parise, J. B.; Zhou, H.-C. *J. Am. Chem. Soc.* **2008**, *130*, 15896−15902.
(13) Ma, S.; Sun, D.; Ambrgio, M.; Fillinger, J. A.; Parkin, S.; Zhou, H.-C. *J. Am. Chem. Soc.* **2007**, *129*, 1858−1859.
(14) Dincă, M.; Dailly, A.; Tsay, C.; Long, J. R. *Inorg. Chem.* **2008**, *47*, 11−13.
(15) Caskey, S. R.; Wong-Foy, A. G.; Matzger, A. J. *J. Am. Chem. Soc.* **2008**, *130*, 10870−10871.
(16) Debatin, F.; Thomas, A.; Kelling, A.; Hedin, N.; Bacsik, Z.; Senkovska, I.; Kaskel, S.; Junginger, M.; Muller, H.; Schilde, U.; Jager, C.; Friedrich, A.; Holdt, H. J. *Angew. Chem., Int. Ed.* **2010**, *49*, 1258−1262.
(17) Rowsell, J. L. C.; Millward, A. R.; Park, K. S.; Yaghi, O. M. *J. Am. Chem. Soc.* **2004**, *126*, 5666−5667.
(18) An, J.; Geib, S. J.; Rosi, N. L. *J. Am. Chem. Soc.* **2010**, *132*, 38−39.
(19) Britt, D.; Furukawa, H.; Wang, B.; Glover, T. G.; Yaghi, O. M. *Proc. Natl. Acad. Sci. U. S. A.* **2006**, *103*, 10186−10191.
(20) Pachfule, P.; Chen, Y.; Jiang, J.; Banerjee, R. *J. Mater. Chem.* **2011**, *21*, 17737−17745.
(21) Prasad, T. K.; Suh, M. P. *Chem.—Eur. J.* **2012**, *18*, 8673−8680.
(22) Yang, S.; Lin, X.; Lewis, W.; Suyetin, M.; Bichoutskaia, E.; Parker, J. E.; Tang, C. C.; Allan, D. R.; Rizkallah, P. J.; Hubberstey, P.; Champness, N. R.; Thomas, K. M.; Blake, A. J.; Schröder, M. *Nat. Mater.* **2012**, *11*, 710−716.
(23) Mulfort, K. L.; Farha, O. K.; Malliakas, C. D.; Kanatzidis, M. G.; Hupp, J. T. *Chem.—Eur. J.* **2010**, *16*, 276−281.
(24) Zhang, S. M.; Chang, Z.; Hu, T. L.; Bu, X. H. *Inorg. Chem.* **2010**, *49*, 11581−11586.
(25) Gu, X.; Lu, Z.; Xu, Q. *Chem. Commun.* **2010**, *46*, 7400−7402.
(26) Lässig, D.; Lincke, J.; Moellmer, J.; Reichenbach, C.; Moeller, A.; Gläser, R.; Kalies, G.; Cychosz, K. A.; Thommes, M.; Staudt, R.; Krautscheid, H. *Angew. Chem., Int. Ed.* **2011**, *50*, 10344−10348.
(27) An, J.; Rosi, N. L. *J. Am. Chem. Soc.* **2010**, *132*, 5578−5579.
(28) Banerjee, R.; Furukawa, H.; Britt, D.; Knobler, C.; O'Keeffe, M.; Yaghi, O. M. *J. Am. Chem. Soc.* **2009**, *131*, 3875−3877.
(29) Llewellyn, P. L.; Bourrelly, S.; Serre, C.; Vimont, A.; Daturi, M.; Hamon, L.; Weireld, G. D.; Chang, J.-S.; Hong, D.-Y.; Hwang, Y. K.; Jhung, S. H.; Férey, G. *Langmuir* **2008**, *24*, 7245−7250.
(30) Demessence, A.; D'Alessandro, D. M.; Foo, M. L.; Long, J. R. *J. Am. Chem. Soc.* **2009**, *131*, 8784−8786.
(31) Farrusseng, D.; Daniel, C.; Gaudillère, C.; Ravon, U.; Schuurman, Y.; Mirodatos, C.; Dubbeldam, D.; Frost, H.; Snurr, R. Q. *Langmuir* **2009**, *25*, 7383−7388.
(32) Wang, Q. M.; Shen, D. M.; Bulow, M.; Lau, M. L.; Deng, S. G.; Fitch, F. R.; Lemcoff, N. O.; Semanscin, J. *Microporous Mesoporous Mater.* **2002**, *55*, 217−223.
(33) An, J.; Geib, S. J.; Rosi, N. L. *J. Am. Chem. Soc.* **2009**, *131*, 8376−8377.